Transparent oxygen optodes in environmental applications at fine scale as measured by luminescence lifetime imaging

Gerhard Holst, Ulrich Franke, Björn Grunwald,
Max-Planck-Institute for Marine Microbiology,
Microsensor Research Group, Bremen, Germany

ABSTRACT

Due to the **mo**dular **l**uminescence **l**ifetime **i**maging system (MOLLI) that has been developed within the last few years, it is possible to use oxygen sensors that are not optically isolated. Transparent planar optodes and dispersed nano-optodes for the first time enable a direct optical link between the chemical parameter to be measured (oxygen as an example) and the structure that is responsible for the distribution of the chemical parameter (ascidian and corals as an example). Since the transparency as a principal quality of the optode allows to record structural images.
The spatial resolution of the MOLLI imaging system is determined by a) the area size of the view field that is imaged onto the amount of pixels of the CCD-chip (640x480 in our case) and b) by the spatial limitations of the sensing layer. The latter means in case of the planar optode the thickness of the sensing layer and in case of dispersed nano-optodes the thickness of the excitation light field. We present biological applications of transparent planar optodes (thickness ≈ 5-10 µm) at two areal resolutions, a) 50 µm / pixel and b) 6 µm / pixel and one application of nano-optodes at 80 µm / pixel. The first application shows the oxygen production of endolithic cells that live in the skeleton of massive corals, measured in a cut coral sample that was illuminated through the planar oxygen optode with defined light energy levels to follow the oxygen production of these coral symbionts. Finally the oxygen production and consumption of coral symbionts are shown by dispersed oxygen nano-optodes in the medium. The specific set-up for the latter experiment will be discussed with the future implication of possible 3D measurements.
Although the results all come from biological applications from coral reef environments, obviously the measuring system and the transparent sensors can be applied to a variety of environmental topics. At the moment similar optodes are under development for parameters like pH, CO_2 and temperature.

Keywords: nano optode, oxygen optode, planar optode, MOLLI, 3D oxygen measurement, non-invasive oxygen measurement, luminescence lifetime imaging,

1. INTRODUCTION

A broad range of publications in the last decade demonstrated, that the two dimensional (2D) imaging of solute distributions with luminescent indicators has become an important tool in medicine, biology and physics. The first described experimental set-ups and image processing systems capable of measuring luminescence lifetimes[3,4,6,7,14-17] were mainly designed and optimised for microscope applications[6,7,15,16,21-24, 30-32]. They measured for example the oxygen distribution in tissue[1-4], oxygen, pH and Ca^{2+} distributions in cells[5,8,9,21-24], oxygen partial pressure on skin surface or oxygen flux into the skin[10,11,33], and oxygen distributions at the sediment water interface[12,13,26-29]. Nevertheless, they lack versatility in application. Therefore, we designed and realised a modular luminescence lifetime imaging system (MOLLI) that allows for a versatile application at various spatial resolutions ranging from 2 µm/pixel (microscope) to 50 µm/pixel and more (macro lens). Together with improvements, concerning dynamics and stability, transparent planar oxygen optodes have been prepared to measure the 2D oxygen distribution and investigate the structure behind the optode, which caused the corresponding oxygen concentration[20,29,30]. Recently oxygen nano-optodes have been developed, that offer the same advantages as the probes encapsulated by biologically localized embedding – PEBBLEs, described by Kopelman and his group[21-24]. Although the preparation is very much different from the PEBBLE process, the advantages are the defined chemical nano environment and the subsequently more stable sensing application compared to the traditional intracellular measurements[6-9,14,15],. Furthermore, the nano optodes with the realtively long luminescence lifetimes enable the use of the MOLLI system. These nano-optodes, together with a new focal approach to restrict the oxygen information in space by an optically shaped excitation light field allowed the first non-invasive three dimensional oxygen measurements around environmentally relevant samples.

*gholst@mpi-bremen.de; phone +49 (0)421 2028 834; fax +49 (0)421 2028 690; http://www.mpi-bremen.de; Max-Planck-Institute for Marine Microbiology, Microsensor Research Group, Celsiusstr. 1, D-28359 Bremen, Germany

2. MATERIAL AND METHODS

2.1. Optical oxygen measurement

2.1.1. Planar optode

The dynamic quenching of luminescence by oxygen is the basis for the measurement of oxygen concentrations and distributions in various systems. The applied sensors have a planar structure with the luminescent indicator embedded in PVC that is spread by a knife coating process on a transparent polyester support foil (Mylar, DuPont, USA). The applied indicator, ruthenium(II)-tris-4,7-diphenyl-1,10 phenantroline perchlorate ($Ru[diph]_3$)[20], is widely used for oxygen measuring purposes. It has a high quantum yield, a long decay or lifetime and its absorption spectrum nearly perfectly overlaps with the emission spectrum of blue LED's and its large Stokes shift with the emission maximum at 605 nm makes it very suitable for luminescence lifetime imaging.
The oxygen optodes are calibrated with a two component model of the Stern-Volmer equation, that was derived and experimentally modified from a two component model published by Carraway et al. 1991[18,19]:

$$\frac{\tau}{\tau_0} = \frac{I}{I_0} = \frac{frac}{(1 - K_{sv} \cdot [O_2])} + (1 - frac)$$

with τ_0, τ - lifetime in the absence of oxygen or with oxygen, I_0, I - luminescence intensity in the absence or with oxygen, K_{sv} - bimolecular quenching coefficient, $[O_2]$ - oxygen concentration in % volume or % air saturation, frac - fractionating factor.

2.1.2. Nano-optodes

To measure oxygen non-invasively in aqeous systems the published approaches were based on solved indicators. But the above mentioned indicator is not soluble in water and the albumin-coupled approach of Wilson and colleagues[1-4] is not suitable in marine systems, since the molecules are too large. Furthermore, to enable the evaluation with MOLLI it is necessary that the luminescence lifetimes to be measured are longer than 500ns (gating limit of the CCD camera). The new approach instead of the immobilisation of the indicator in nano-spheres of polyacrylamide, is based on the electrostatical coupling of the indicator ruthenium(II)-tris-4,7-diphenyl-1,10 phenantroline to the polyelectrolyte polysulfonic acid. These conjugates have a molecular weight of appr. 100 000 and they are at the limit to be treated as solution or dispersion. The calibration uses the same experimentally modified two component model of the Stern-Volmer equation (see above). If these nano-optodes are put into the test liquid, like salt water, after stirring of 2 minutes the liquid volume seems to be dyed, is macroscopically it looks like a solution.

2.2. MOLLI - Imaging system

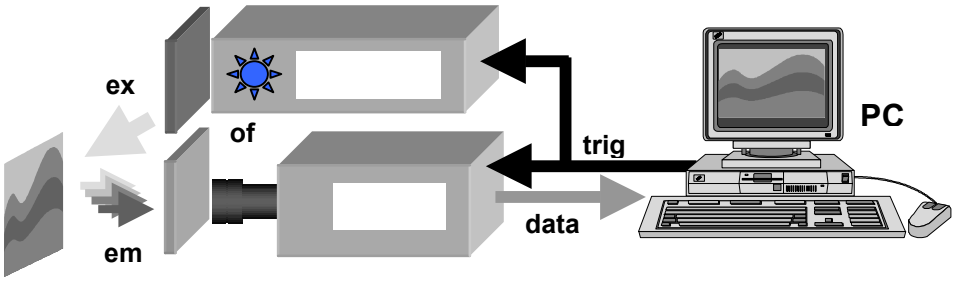

Figure 1: Schematical overview on the **mo**dular **l**uminescence **l**ifetime **i**maging system – MOLLI. The personal computer (PC) controls with the timing signals the excitation light source (ex-light) and the modulated fast shutter CCD-camera (CCD). The excitation light passes an appropriate optical filter (of) and excites the planar or the nano-optode (ex). The emitted luminescence (em) passes an appropriate emission filter (of) and is detected by the CCD-camera (CCD). Finally the images are read out (data) by the PC.

The MOLLI imaging system (Fig. 1) consists of an electrically cooled CCD-camera (SensiMod, PCO Computer Optics, Kehlheim, Germany) with a fast electronical shutter feature. Additionally, the camera has a specially customized

modulation input to directly control the fast shutter (ton = 500 ns and toff = 500 ns, maximum modulation frequency 1 MHz). The camera (dynamic range 12 = Bit, resolution 640x480 pixel) is connected via a serial fiberoptical link to a camera control PCI-board in a Pentium based PC (Fig. 2, PC). The PC controls image acquisition, storage, display and timing. For the precise timing of excitation light source switching and image acquisition, the PC has a special software controlled timing board inserted (PADCO-06, Spectrum Systementwicklung Microelectronic, Bültbek, Germany) that generates the necessary timing signals (Fig. 1, trig). Timing control and primary image acquisition was programmed in Delphi 5 (Delphi 5, Borland, Scotts Valley, USA), while the image processing and visualization were programmed in IDL 5.4 (Research Systems Inc., Boulder, USA). For planar optode applications, the excitation light source consisted of a frame of 20 LED's (HLMP-CB15, Hewlett Packard, USA), whose light was coupled through holographic diffusers (Physical Optics Corporation, Torrance, CA, USA) onto the optode. The LEDs are driven by a specially developed driving circuit, that is triggered by the timing board in the PC. For the nano-optode application, the excitation light was a laserdiode module (PVLS-3000-MPIMM, lp=404 nm, Toptica Photonics, Martinsried, Germany) with a monomode fiber pigtail that was connected to a lineoptic module (OZ Optics, Ontario, Canada), generating a laserline of approximately 200µm or less thickness.

2.3. Timing of image acquisition

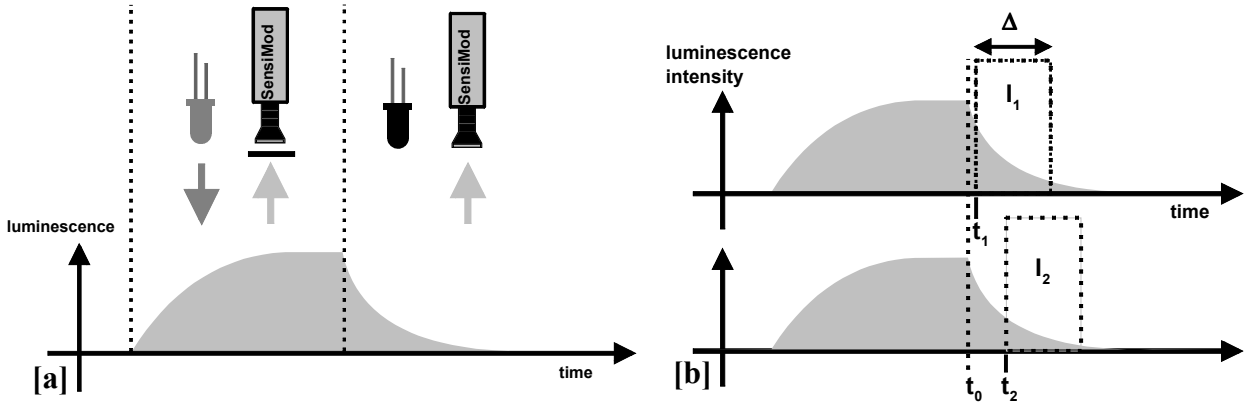

Figure 2: [a]: Image acquisition timing scheme for luminescence lifetime imaging. The given luminescence signal vs. time corresponds to the light signal that is detected by each pixel of the CCD-chip. The timing starts with excitation light ON and the camera shutter closed, the luminophore absorbs light and luminescence is emitted. Then the excitation light is switched OFF and the camera shutter is opened. This is repeated numerous times during the overall camera "integration" time.
[b] Scheme to calculate the corresponding lifetime images from recorded images. All detected images have the same width Δ and integrate the intensity I_i of the decay curve. Each window has a different delay t_i compared to the switch OFF time of the excitation light. The window "open" operation is repeated several times for the same delay t_i to integrate the light information on the CCD chip.

Figure 2 [a] shows the detection principle that is applied for each pixel. First the excitation light source is switched ON e.g. for 4 µs and illuminates the planar optode or the nano-otpodes. The luminescence that is detected by each pixel rises until a steady state between absorbed and emitted energy of the dye molecules is reached (Fig. 2 [a], time course of the luminescence signal). Then the light source is switched OFF and appr. 0.5 µs later the camera shutter is opened, allowing ambient light and luminescence to reach the CCD chip for a certain time window e.g. 3 µs. This series of events is repeated for maybe 10 000 times, while the incident light is integrated on the CCD chip before the image is passed to the PC. For further improvement of the signal to noise ratio, the procedure can be repeated a couple of times to perform an efficient averaging. After the recording of the 2 images, an image is recorded without the excitation to measure the background light, that directly can be subtracted from the measured images to prevent the ambient light information in the images from being further processed.

2.4. Evaluation of lifetime images

To evaluate the corresponding lifetime of the light information detected by each pixel, two images are recorded, where each image is acquired with a different delay time t_i relative to the switch OFF event of the excitation light source (Fig. 2 [b]). The basic model assumption is, that the decay curve follows a monoexponential decay. Many investigations have shown, that in principle 4 or more lifetimes can be best fitted to a recorded decay curve of such a sensor. But for practical sensing applications; the assumption of a single, so called apparent lifetime, seems to be justified (as can be seen by the comparison of raw data and model fit in figure 6).
The images are processed based on this assumption. The two images (i = 1,2) (Fig. 2 [b]) with a time interval Δ_i have their delay t_i compared to the excitation light OFF event. To receive enough light intensity each image represents the integral over a number, n_i, of illumination events. The measured images S_i are stored after subtraction of the dark image. The intensity of one image is given by:

$$I_i = \frac{S_i}{n_i}, i = 1,2$$

The intensity, as dependent on the apparent lifetime τ, can be described by the following equation:

$$I_i = I_0 \cdot \tau \cdot \exp\left(\frac{t_i}{\tau}\right) \cdot \left[1 - \exp\left(-\frac{\Delta_i}{\tau}\right)\right]$$

with the unknown intensity I_0 at the time t_0 when the excitation light is switched OFF. As the image collection uses a constant detection window width:

$$\Delta_1 = \Delta_2 = \Delta$$

The further image processing is reduced to:

$$\tau = \frac{(t_2 - t_1)}{\ln(S_1/S_2)}$$

If the further reduction of noise is necessary, it is possible to increase the number of windows and average the lifetime results, but in our applications the 2 window approach was sufficient.

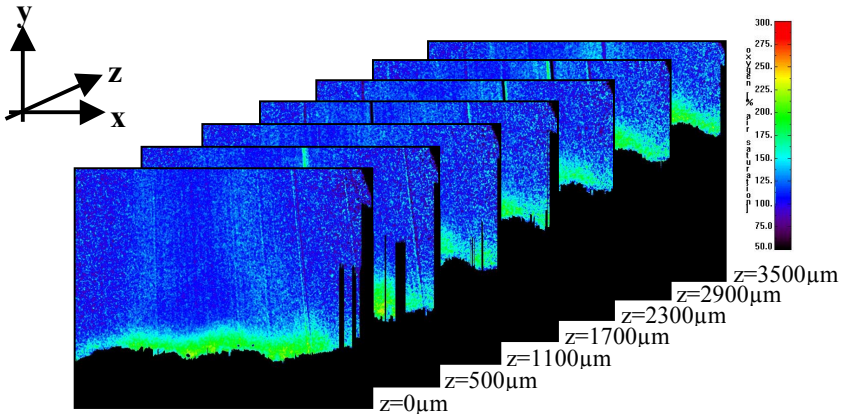

Figure 3: Sequentially recorded 2D oxygen images at various positions (z). While the spatial resolution in the xy-planes (in each image) is 17.2 µm/pixel, the depth resolution in z-direction is 100 µm. The colorbar shows the color coding of the oxygen values. The coordinate system defines the overall used axis directions.

2.5. 3D image recording

There are in principle two possibilities to restrict the information of the two dimensional (2D) optical oxygen measurement spatially to a thin slice. First, the planar optode, whose thickness is small compared to the horizontal spatial resolution of the measurement (10 µm vs. 40µm/pixel). So the spatial resolution in depth is reached by a spatial limitation of the indicator. Second, if equally distributed nano-optodes are applied, the spatial limitation can be achieved either by a confocal detection principle[30-32] or by an appropriate shaping of the excitation light field.
For our work the excitation light, coming from a laser diode, was shaped by line optics to generate a laser line of appr. 200µm. The line optics have an adjusted fixed distance to the camera, so the camera is once focussed to the light sheet and both are moved simultaneously, so there no further focussing is necessary. This allowed a sequential recording of 2D oxygen distribution images, with each image at another depth position (Fig. 3). These sets of "oxygen" images represent a 3D data volume that can be processed in various ways (Fig. 8).

3. EXPERIMENTAL SETUPS & RESULTS

3.1. Experimental setups

3.1.1. Calibration measurements and concentration of nano-optodes

A concentrated solution of nano-optodes was diluted in saltwater at 3.5% salinity. The solution was pumped from a reservoir bottle through a small glass chamber with planar glass walls. The closed chamber had the in and out-flow connection in the top plate. It was illuminated by the laser light from the side. The water dye solution in the reservoir bottle was continuously perfused by a nitrogen – oxygen gas mixture that was controlled by a gas mixing pump. The bottle was closed by parafilm to enable the gas to emerge through the top. As the reservoir was continuously perfused, after approximately 20 minutes a steady state of the gas concentration within the liquid was reached and images were recorded. This was repeated for different gas concentrations and different dilutions. For evaluation of the luminescence lifetimes a 10x10mm² area within the illuminated area was used to calculate mean and standard deviation of the lifetime. These lifetimes for each dilution stage have been fitted with the above described model (Fig. 6, table 1).

3.1.2. Transparent planar oxygen optode

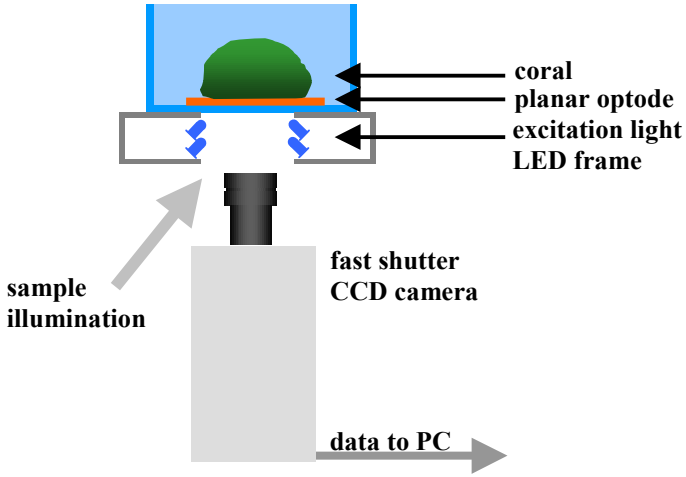

Figure 4: Schematic of experimental setup for experiments with planar oxygen optodes. The sample, a cutted massive coral, *Porites,* was placed on top of the transparent planar oxygen optode, that was fixed at the bottom of a transparent glass container. The container, filled with water from the sampling site, was hold by the excitation light LED frame. The optode was imaged to the CCD chip by a macro lens through the frame. For sunlight simulation at defined light energy levels the coral was illuminated through the bottom of the glass container (sample illumination).

To investigate the productivity of endolithic cells that live within the skeleton of massive corals, the planar oxygen optode was placed at the bottom of a glass vessel, filled with seawater from the place where the coral sample was taken

(Heron Island Lagoon, Great Barrier Reef, Queensland, Australia). Subsequently the cut piece of *Porites* was placed with the fresh surface on top of the optode and left there for 2 hours to equilibrate and settle in the darkness. The vessel stood on the LED frame (Fig. 4). The CCD camera was mounted on a tripod pointing upward (Fig. 4). A sunlight simulating light source (not drawn in figure 4, swan neck halogen lamp) was positioned at the side of the camera, to enable illumination of the endolithic cells through the transparent optode at various light energy levels. The illumination was adjusted at the lamp. The coral was illuminated at each level for about 45 minutes. Then the illumination was switched off, and lifetime images were recorded every 2 s (for 2 minutes). Subsequently images were recorded every 15 s (for 3 minutes). Then the next higher light level was selected and the lamp was switched on again. At the end of the experiments the coral was removed, and the water volume was saturated first with nitrogen and second with air to obtain calibration images. The sunlight simulating light source was calibrated by measuring directly above the planar optode within the water with a light energy meter (Biospherical, USA). The adjusted light energy levels are given in table 1. The converted visualisation images of the 2D oxygen distribution correspond to the situation after switching off the sunlight simulation at each level. The result images are blended onto a black & white image, that has been taken through the planar optode (Figure 7).

3.1.3. Non-invasive and 3D oxygen measurement with nano-optodes

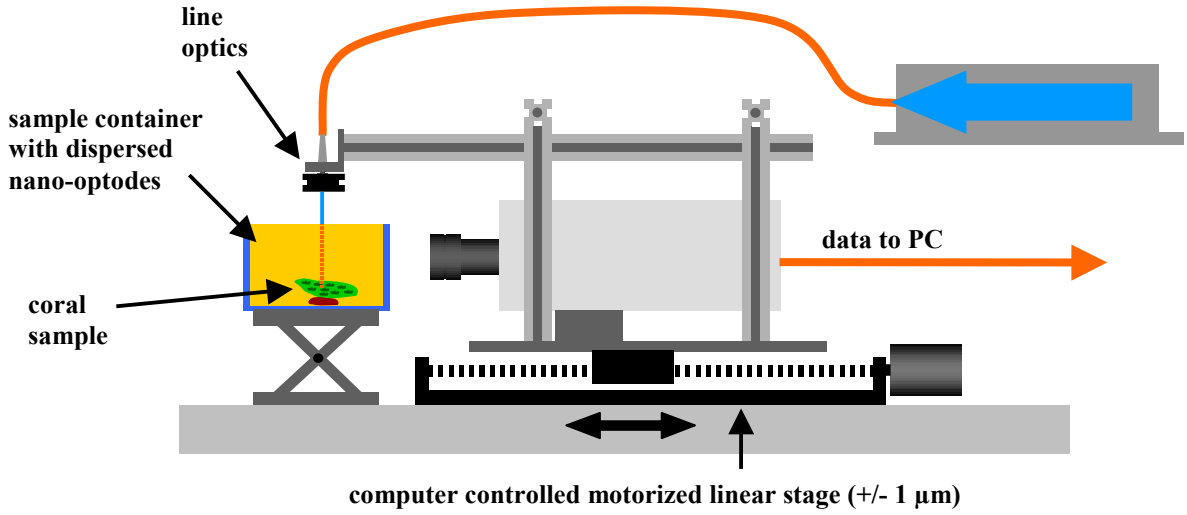

Figure 5: Schematic of 3D experiments with oxygen nano-optodes. The CCD camera and the line optics for the excitation light beam of the laser diode were mounted into the same aluminium frame, itself fixed on a linear stage. The linear stage is motorized, computer controlled, and capable of moving with a unidirectional precision of +/- 1 µm with an absolute travel range of 300mm. The coral sample, *Acropora,* was placed in a salt water filled transparent sample container with a dispersion of oxygen nano-optodes. The excitation light (λ_{peak}=404nm, 8mW at fiber output) from the laserdiode module was coupled into the line optics with a quartz monomode fiber.

As can bee seen in figure 5, the CCD camera and the line optics connected to the monomode fiber, which is attached to the excitation light laser diode, are mounted within the same frame setup made of aluminum bars. Base plate and frame are mounted on the movable stage of a computer controlled motorized linear stage, capable of moving at an unidirectional accuracy of +/- 1 µm (VT-80, Micos, Umkirch, Germany). After focussing the camera lens onto the light sheet, which is generated by the line optics if the laser diode is on, the setup of camera and light can be moved forward and backward at micrometer travel prescision without refocussing (if the effect of diffraction can be neglected).
A sample container filled with a nano-optode dispersion in seawater at 3.5 % salinity, was positioned in front of the camera frame. A coral sample of cultivated *Akropora* was placed in the container in a such a way, that the backward pointing part (as seen from the camera, in figure 5 pointing to the left) was at a little higher position than the forward pointing part. This resulted in a reasonable increase in height (see rise in surface line in figure 8 [d]). The measure was done to prevent self-shadowing by the surface topography or the coral polyps. For the measurements the coral sample was illuminated by a sunlight simulating halogen lamp for about 45 minutes. Then at each position one 2D oxygen images was recorded. Before the recording the sunlight simulation was interrupted for the measurement, and after the

frame was moved forward. The total traveling range was 35 mm at 100 µm stepwidth, resulting in 36 individual 2D oxygen images. After the oxygen measurements were recorded, black & white images (without emission filter) were recorded at the same positions, as before, to image the laser line, which indicates the surface of the sample. These images were processed with a maximum determination to evaluate the position of the surface in the images. This information was subsequently introduced into the 2D oxygen images and used to cut off any artificial oxygen information below the surface line (that is generated by reflection and scattering of fluorescence before the light sheet). The final result is a data set of 2D oxygen distribution images (Fig. 8, xy-plane) above the sample surface, where each image represents a spatial depth average of approximately 100 µm (Fig. 8, z-direction). The series of measured images form a 3D data volume with the spatial dimensions x*y*z (11*8.25*35mm³), which corresponds to a pixel resolution of 17.2 µm/pixel in the xy-plane and 100µm in z-direction.

3.2. Results

3.2.1. Calibration measurements and concentration of nano-optodes

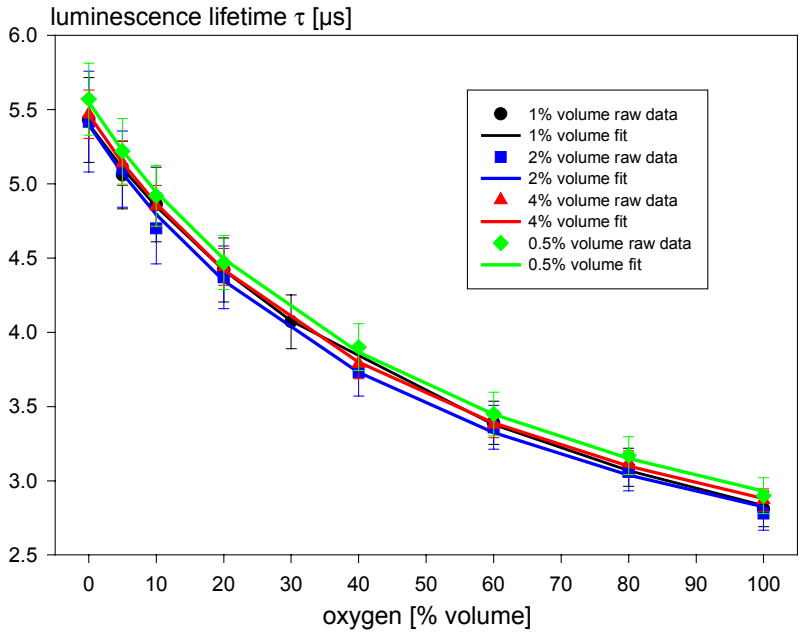

Figure 6: Raw data and fit curves of calibration experiments with oxygen nano-optodes (luminescence lifetimes, as measured by MOLLI, vs. oxygen concentration) and nano-optode concentration as parameter (given in percentage of total volume of saltwater)

The calibration curves that have been fitted (Fig. 6) were in excellent agreement with the raw data within the given standard deviations.

Table 1: Fit results of calibration experiments according to the model in 2.1.1.

nano-optode concentration [% volume]	zero oxygen lifetime τ_0 [µs]	quenching coefficient K_{SV} [(% volume oxygen)$^{-1}$]	fraction of quenchable luminescence	correlation coefficient
0.5	5.5496	0.017	0.75	0.9997
1	5.402	0.0148	0.796	0.9997
2	5.398	0.0176	0.748	0.9989
4	5.465	0.0172	0.748	0.9998

These deviations were caused by scattered laser light, due to bubbles and water movements in the experimental chamber. But there is no direct relation visible between the fit parameters and the concentration of the nano-optodes. The fitted parameters are in good agreement with each other (table 1). Although every fit has an excellent correlation coefficient, the deviation at the concentration of 2% maybe explained with selection of 30 % volume oxygen instead of 40 % oxygen like the other measurements, because oxygen concentration values in that range have some influence on the curvature. Further measurements with various delays of the measuring windows (see 2.3 and 2.4) showed nearly constant lifetime values in the images. This indicates that the assumption of a single or mono-exponential decay behavior is justified.

3.2.2. Transparent planar oxygen optode

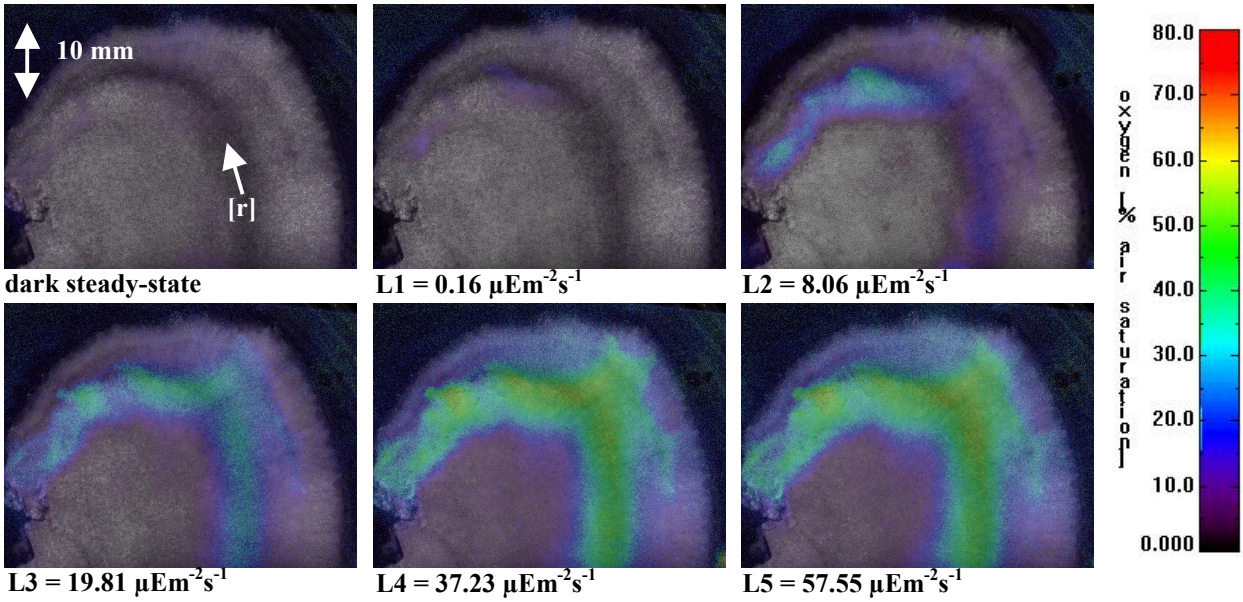

Figure 7: 2D oxygen distribution images blended into a black & white image of the coral, seen through the optode. The oxygen images were recorded after switching off the illumination of the coral through the optode at different light energy levels (L1-L5). Oxygen values were given in % air saturation and color coded between 0 – 80 % as. The dark ring [r] in the structure image represents the position of the endolithic cells.

The 2D oxygen distribution images obtained with the planar optodes nicely demonstrate the activity of the endolithic cells, that live within the coral skeleton. While the other symbionts like *zooxanthellae*, which live in the outer tissue of the coral can be investigated with microsensors, the endolithic cells are not accessible with this technology. In their natural habitat these cells are adapted to small light energy levels, because only small amounts light are able to penetrate the tissue layer and the skeleton, since most of the energy is absorbed and used by the algae in the outer tissue. The outer light energy level on a sunny day may rise up to 1500 $\mu Em^{-2}s^{-1}$ or even more. In contrast to this light situation, the endolithic cells start to produce oxygen significantly from L2 = 8.06 $\mu Em^{-2}s^{-1}$. The link to the endolithics is given by the position of the increased oxygen layers on top of the dark ring that is visible in the structure below, which represents the position of the endolithic cells. With these measurement the productivity of the cells can be estimated.

3.2.3. Non-invasive and 3D oxygen measurement with nano-optodes

With the specially developed image processing software "MolliView" (written in IDL, RSI, Colorado, USA) the recorded images can be loaded to form a 3D data volume. Surface lines have determined and used to mask out any non-relevant oxygen information below that line. Within the data volume arbitrary planes can be selected to investigate local oxygen concentrations and gradients. Figure 8 [a] – [d] shows some examples. As starting plane the xy – plane oxygen distribution at position z = 1800 µm from the start is shown in figure 8 [a]. The grey scale coding of the oxygen range is

stretched from 80 to 300 % air saturation (Fig. 8 [e]). The oxygen distribution above the surface shows oversaturation above the coral surface, due to the photosynthesis of the symbionts. The area in the xy-plane corresponds to 11000 µm x 8250 µm. The white line at a height of y = 3685 µm is the line selected for a display of the oxygen distribution in the xz-plane, shown in figure 8 [b]. The line crosses the coral surface in the right part of the image. This surface line like a height line appears in the xz-plane oxygen distribution (Fig. 8 [b]) as dark area above the oxygen values. The xz-plane shows an area of 11000 µm x 3500 µm, while the white line shows the position of the first image in the xz-plane. It is nicely visible the brighter area of oxygen oversaturation along the increasing coral sample ridge.

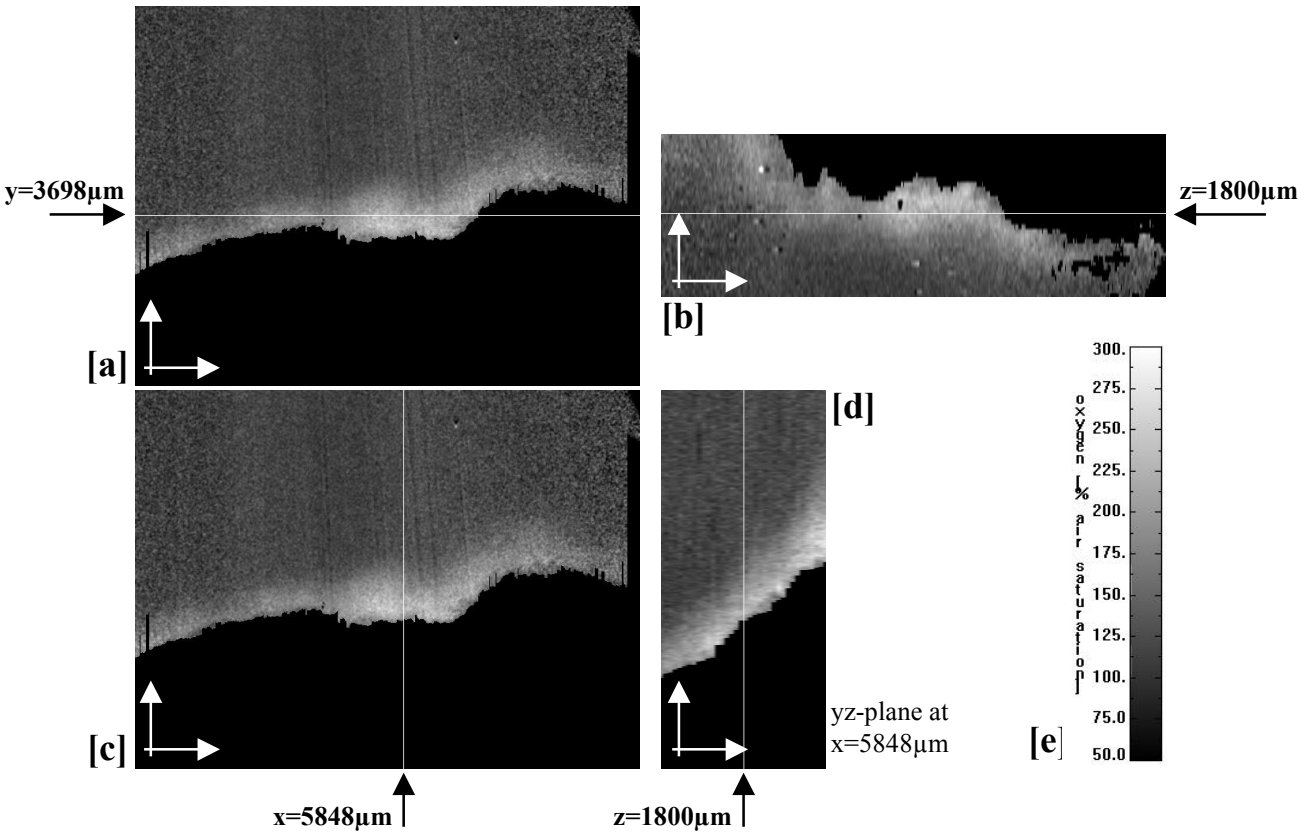

Figure 8: 2D images from a 3D data set of 36 single 2D oxygen images from position z = 0 µm to z = 3500 µm.
[a] 2D oxygen distribution at position z = 1800 µm (xy-plane), the horizontal line at y = 3698 µm indicates the position of the xz-plane shown in (b).
[b] 2D oxygen distribution at position y = 3698 µm (xz-plane), image is stretched to have the same spatial dimensions like the xy-planes in (a) and (c), the horizontal line at z = 1800 µm shows the position of the xy-plane in (a).
[c] 2D oxygen distribution at position z = 1800 µm (xy-plane), the vertical line at x = 5848 µm indicates the position of the yz-plane shown in (d).
[d] 2D oxygen distribution at position x = 5848 µm (yz-plane), image is stretched to have the same spatial dimensions like the xy-planes in (a) and (c), the vertical line at z = 1800 µm shows the position of the xy-plane in (c).
[c] greyscale bar with the oxygen coding of the images.

Figure 8 [c] is the same starting plane like figure 8 [a], only that this time the white line indicates the position of the extracted yz-plane in figure 8 [d] at the horizontal position of x = 5838 µm. The yz-plane gives the profile of the coral surface topography. It nicely shows the oversaturation along the coral surface and displays an area of 3500 µm x 8250 µm. Therefore a 3D map of the oxygen distribution above the coral surface can be created and different investigations of corals as monitors of environmental parameters can be performed. Corresponding dark steady state measurements have been made and showed the expected oxygen consumption in the dark (data not shown).

4. DISCUSSION

The 2D measurement of the oxygen distribution by luminescence lifetime imaging with MOLLI enable for the first time the direct link between the local oxygen concentration and the structure where it is generated. The results prove the quality of the measurement. For the first time it was possible to monitor and measure the oxygen production by endolithic cells within the skeleton of massive corals to obtain more insight in this balanced system of symbionts. Nevertheless, even in this successful application, fast repetition rates for the image uptake are not favourable, because the inherent excitation light, which passes the optode, may generate oxygen on its own. This happens if the high repetition rate creates an average illumination level. However, this is only a problem in photosynthecially active systems.

The nano-optodes with the spatially restricted excitation represents one of the first 3D oxygen measurements in aqueous samples. Although there have been applications with dissolved or dispersed indicators, the spatial relation was only used in some confocal microscopical applications. The application is limited by the following parameters. First, the transparency of the liquid including the amount of scattering particles, which, if they move between the two recorded images, result in artificial lifetimes, influencing localized measurements. Second, the visibility of the light sheet is important, since object morphology may shadow or mask the light and simply prevents the uptake of a useful luminescence lifetime image. Furthermore, the influence of the nano-optodes on the biological system in long-term applications has to be investigated. Beside these limitations, the non-invasive 3D oxygen measurement in transparent aquatic environments open a broad range of new experimental schemes for applications to investigate environmentally relevant organisms, i.e., which are indicators for the ecological condition of reef systems and sensitively respond to worlds climate changes. Furthermore new detection schemes like time domain dual lifetime referencing[28] can be applied to these transparent optodes as well, opening the fields of application to parameters like pH and carbon dioxide[28,33].

5. ACKNOWLEDGEMENTS

The authors would like to thank Ingo Klimant (Technical University, Graz, Austria) and Christian Krause (PreSens Precision Sensing GmbH, Regensburg, Germany) for providing the planar optodes and the nano-optodes and fruitful discussions about the results. They furthermore want to thank Peter Ralph (University of Technology, Sydney, Australia) for the endolithic cells experiments and the *Porites* sample and Christian Wild (Max-Planck-Institute for Marine Microbiology) for the Akropora sample. Furthermore they would like to acknowledge the financial support of the BMBF project F0284 "OPTIONS" of the Germany ministery of research and education and the Max-Planck-Society.

6. REFERENCES

1. W.L. Rumsey, J.M. Vanderkooi, and D.F. Wilson, "Imaging of Phosphorescence: a Novel Method for Measuring Oxygen Distribution in Perfused Tissue", Science 241, pp. 1649-1651, 1988.
2. W.L. Rumsey, R. Iturriaga, D.F. Wilson, S. Lahiri, and D. Spergel, "Phosphorescence and Fluorescence Imaging: New Tools for the Study of Carotid Body Function", in Chemoreceptors and Chemoreceptor Reflexes, pp. 73-79, Plenum Press, New York, 1990.
3. R.D. Shonat, D.F. Wilson, C.E. Riva, and M. Pawlowski, “Oxygen Distribution in the Retinal and Choroidal Vessels in the Cat as Measured by a New Phosphorescence Imaging Method”, Appl. Opt. 31, pp. 3711-3718, 1992.
4. S. Vinogradov, L.-W. Lo, W.T. Jenkins, S.M. Evans, C. Koch, and D.F. Wilson, “Noninvasive Imaging of the Distribution in Oxygen in Tissue In Vivo Using Near-Infrared Phosphors”, Biophys. J. 70, pp. 1609-1617, 1996.
5. S. Nomura, M. Nakao, T. Nakanishi, S. Takamastu, and K. Tomita, “Real Time Imaging of Microscopic pH Distribution with a Two-Dimensional pH-Imaging Apparatus”, Anal. Chem. 69, pp. 977-981, 1997.
6. J.R. Lakowicz and K.W. Berndt, "Lifetime-Selective Fluorescence Imaging Using a RF Phase Sensitive Camera", Rev. Sci. Instrum. 62, pp. 1727-1734, 1991.
7. J.R. Lakowicz, H. Szmacinski, K. Nowaczyk, K.W. Berndt, and M. Johnson, "Fluorescence Lifetime Imaging", Anal. Biochem. 202, pp. 316-330, 1991.
8. N. Opitz, E. Merten, and H. Acker, “Evidence for redistribution-associated intracellular pK shifts of the pH-sensitive fluoroprobe carboxy-SNARF-1”, European Journal of Physiology 427, pp. 332-342, 1994.
9. N. Opitz, T. Porwol, E. Merten, and H. Acker, “On The Protein-Error Of The Calcium-Sensitive Fluorescent Indicator Fura-Red,” in Fluorescence Microscopy and Fluorescence Probes, J. Slavik, Ed. New York: Plenum Press, pp. 101-106, 1996.
10. P. Hartmann and W. Ziegler, "Lifetime Imaging of Luminescent Oxygen Sensors Based on All-Solid-State Technology", Anal. Chem. 68, pp. 4512-4514, 1996.

11. P. Hartmann, W. Ziegler, G. Holst, and D.W. Lübbers, "Oxygen Flux Fluorescence Lifetime Imaging", Sensors and Actuators B 38-39, pp. 110-115, 1997.
12. R.N. Glud, N.B. Ramsing, J.K. Gundersen, and I. Klimant, “Planar Optrodes: A New Tool for Fine Scale Measurements of Two-Dimensional O2 Distribution in Benthic Communities”, Mar. Ecol. Prog. Ser. 140, pp. 217-226, 1996.
13. R.N. Glud, M. Kühl, O. Kohls, and N.B. Ramsing, "Heterogeneity of Oxygen Production and Consumption in a Photosynthetic Microbial Mat as Studied by Planar Optodes", J. Phycol. 35, pp. 270-279, 1999.
14. C.G. Morgan, A.C. Mitchell, and J.G. Murray, "Fluorescence Decay Time Imaging Using an Imaging Photon Detector with a Radiofrequency Photon Correlation System", in Conference on Time-Resolved Laser Spectroscopy in Biochemistry II, Proc. SPIE, pp. 798-807, 1990.
15. G. Marriott, R.M. Clegg, D.J. Arndt-Jovin, and T.M. Jovin, "Time Resolved Imaging Microscopy", Biophys. J. 60, pp. 1374-1387, 1991.
16. R.M. Clegg, B. Feddersen, E. Gratton, and T.M. Jovin, "Time Resolved Imaging Fluorescence Microscopy", Conference on Time-Resolved Laser Spectroscopy in Biochemistry II, Proc. SPIE, pp. 448-460, 1990.
17. X.F. Wang, T. Uchida, D.M. Coleman, and S. Minami, “A Two-Dimensional Fluorescence Lifetime Imaging System Using a Gated Image Intensifier”, Appl. Spec. 45, pp. 360-366, 1991.
18. E.R. Carraway, J.N. Demas, B.A. DeGraff, and J.R. Bacon, "Photophysics and Photochemistry of Oxygen Sensors Based on Luminescent Transition-Metal Complexes", Analytical Chemistry 63, pp. 337-342, 1991.
19. E.R. Carraway, J.N. Demas, and B.A. DeGraff, "Luminescence Quenching Mechanism for Microheterogeneous Systems", Analytical Chemistry 63, pp. 332-336, 1991.
20. I. Klimant, P. Belser, and O.S. Wolfbeis, "Novel Longwave Absorbing and Emitting Transition Metal Complexes for Use in Optical Oxygen Sensing", Europt(r)ode I, Graz, 1, 1992.
21. H. A. Clark, S. L. R. Barker, M. Brasuel, M. T. Miller, E. Monson, S. Parus, S. Zhong-You, A. Song, B. Thorsrud, R. Kopelman, A. Ade, W. Meixner, B. Athey, M. Hoyer, D. Hill, R. Lightle, and M. A. Philbert, “Subcellular optochemical nanobiosensors: probes encapsulated by biologically localised embedding (PEBBLEs),” Sensors and Actuators B, vol. 51, pp. 12-16, 1998.
22. H.A. Clark, M. Hoyer, M.A. Philbert, and R. Kopelman, "Optical Nanosensors for Chemical Analysis inside Single Living Cells. 1. Fabrication, Characterization, and Methods for Intracellular Delivery of PEBBLE Sensors", Analytical Chemistry 71, pp. 4831-4836, 1999.
23. H.A. Clark, M. Hoyer, M.A. Philbert, and R. Kopelman, "Optical Nanosensors for Chemical Analysis inside Single Living Cells. 2. Sensors for pH and Calcium and the Intracellular Application of PEBBLE Sensors", Analytical Chemistry 71, pp. 4837-4843, 1999.
24. H. Xu, J.W. Aylott, R. Kopelman, T.J. Miller, and M.A. Philbert, "A Real-Time Ratiometric Method for the Determination of Molecular Oxygen inside Living Cells Using Sol-Gel-BAsed Spherical Optical Nanosensors with Applications to Rat C6 Glioma", Analytical Chemistry 73, pp. 4124-4133, 2001.
25. G. Holst, O. Kohls, I. Klimant, B. König, M. Kühl, and T. Richter, "A modular luminescence lifetime imaging system for mapping oxygen distribution in biological samples", Sensors and Actuators B 51, pp. 163-170, 1998.
26. G. Holst, B. Grunwald, I. Klimant, and M. Kühl, "A Luminescence Lifetime Imaging System USing Imaging Fibers to Measure the 2D Distribution of O_2 in Biological Samples", Proceedings of Fiber Optic Sensor technology and Application, SPIE Vol. 3860, pp. 154-163, 1999.
27. G. Holst, and B. Grunwald, "Luminescence lifetime imaging with transparent oxygen optodes", Sensors and Actuators B 74, pp. 78-90, 2001.
28. G. Liebsch, I. Klimant, C. Krause, and O.S. Wolfbeis, "Fluorescent Imaging of pH with Optical Sensors Using Time Domain Dual Lifetime Referencing", Analytical Chemistry 73, pp. 4354-4363, 2001.
29. P.J. Verveer, M.J. Gemkow, and T.M. Jovin, "A comparison of image restoration approaches applied to three-dimensional confocal and wide-field fluorescence microscopy", Journal of Microscopy 193, pp. 50-61, 1999.
30. A. Squire, and P.I.H. Bastiaens, "Three dimensional image restoration in fluorescence lifetime imaging microscopy", Journal of Microscopy 193, pp. 36-49, 1999.
31. P.I.H. Bastiaens, and A. Squire, "Fluorescence lifetime imaging microscopy: spatial resolution of biochemical processes in the cell", Trends in Cell Biology 9, pp. 48-52, 1999.
32. K. Carlsson, A. Liljeborg, R.M. Andersson, and H. Brismar, "Confocal pH imaging of microscopic specimens using fluorescence lifetimes and phase fluorometry: influence of parameter choice on system performance", Journal of Microscopy 199, pp. 106-114, 2000.
33. G. Liebsch, I. Klimant, B. Frank, G. Holst, and O. S. Wolfbeis, “Luminescence Lifetime Imaging of Oxygen, pH and Carbon Dioxide Using Optical Sensors,” Applied Spectroscopy 54, pp. 548-559, 2000.